A Hierarchical Image Matting Model for Blood Vessel Segmentation in Fundus Images

D. Vijendra Kumar[1] | K.N.S.Harshita[2] | R.Prasanna[3] | Y. Anjani praneeth [4] | Ch.Rajesh[5]

[1,]Assistant Professor, Department of Electronics and Communication Engineering, Godavari Institute of Engineering and Technology (A), Rajahmundry, Andhra Pradesh, India

[2,3, 4, 5,]UG Students, Department of Electronics and Communication Engineering, Godavari Institute of Engineering and Technology (A), Rajahmundry, Andhra Pradesh, India.

Abstract: In this paper, a hierarchical image matting model is proposed to extract blood vessels from fundus images. More specifically, a hierarchical strategy is integrated into the image matting model for blood vessel segmentation. Normally the matting models require a user specified trimap, which separates the input image into three regions: the foreground, background and unknown regions. However, creating a user specified trimap is laborious for vessel segmentation tasks. In this paper, we propose a method that first generates trimap automatically by utilizing region features of blood vessels, then applies a hierarchical image matting model to extract the vessel pixels from the unknown regions. The proposed method has low calculation time and outperforms many other state-of-art supervised and unsupervised methods. It achieves a vessel segmentation accuracy of 96.0%, 95.7% and 95.1% in an average time of 10.72s, 15.74s and 50.71s on images from three publicly available fundus image datasets DRIVE, STARE, and CHASE DB1, respectively.

Index Terms—Image matting, hierarchical strategy, fundus, trimap, region features, segmentation.

DOI of the Article: https://doi.org/10.46501/GIETEC07

Available online at: https://ijmtst.com/icetee2021.html

As per UGC guidelines an electronic bar code is provided to seure your paper

To Cite this Article: D. Vijendra Kumar; K.N.S.Harshita; R.Prasanna, Y. Anjani praneeth and Ch.Rajesh. A Hierarchical Image Matting Model for Blood Vessel Segmentation in Fundus Images. *International Journal for Modern Trends in Science and Technology* 2021, *7*, pp. 36-40. https://doi.org/10.46501/GIETEC07

Article Info. Received: 18 May 2021; Accepted: 25 June 2021; Published: 30 June 2021

INTRODUCTION

RETINAL blood vessels generally show a coarse to fine recentrifugal distribution and appear as a wire mesh like structure or tree-like structure [1]. Their morphological features, such as length and width, is of great importance in the early detection and therapy of different angiocardiopathy and ocular diseases such as stroke, vein occlusions, diabetes and arteriosclerosis [2]–[4]. The analysis of morphological features of retinal blood vessels is conducive to detecting and treating a disease in time when it is still in its early stage. Since angiocardiopathy and ocular diseases have a serious impact on human's life, the analysis of retinal blood vessels is of great significance in many clinical applications to reveal important information of systemic diseases and support diagnosis and Zhun Fan is a Full Professor with the School of Electrical and Information Engineering, Shantou University, Shan'tou 515063, China. Zhun Fan and Jiewei Lu are with the Guangdong Provincial Key Laboratory of Digital Signal and Image Processing, College of Engineering, Shantou University, Shan'tou 515063, China (email: zfan, 12jwlu1@stu.edu.cn). Caimin Wei is with the Department of Mathematics, Shantou University, Shan'tou 515063, China (email: cmwei@stu.edu.cn). Han Huang is with the School of Software Engineering, South China University of Technology, Guang'zhou 510006, China (email: hhan@scut.edu.cn). Xinye Cai is with the College of Computer Science and Technology, Nanjing University of Aeronautics and Astronautics, Jiang'su 210016, China (email:xinye@nuaa.edu.cn). Xinjian Chen is a Distinguished Professor with the School of Electrical and Information Engineering, Soochow University, Suzhou, 215006, China. He is also with the State Key Laboratory of Radiation Medicine and Protection, Soochow University, Suzhou, 215123, China (email: xjchen@suda.edu.cn). ∗ indicates the corresponding author. treatment. As a result, the requirement of vessel analysis system grows rapidly, in which vessel segmentation is the first and one of the most crucial steps. Vessel segmentation has become an important research field in recent years [5]. Broadly speaking, existing vessel segmentation approaches include two categories: supervised and unsupervised. In supervised methods, a number of different features are extracted from fundus images, and applied to train the effective classifiers with the purpose of extracting retinal blood vessels. In [6], Staal et al. extract 27 features for each image pixel with ridge profiles, and perform feature selection by using sequential forward selection method to choose the pixels that can generate better segmentation performance by a K-Nearest Neighbor classifier. Soares et al. [7] introduce a feature-based Bayesian classifier with Gaussian mixtures, which makes use of the intensity information and Gabor wavelet transform responses to build a 7-D feature vector for each pixel. In [8], Lupascu et al. train an AdaBoost classifier with 41 features which incorporates various structure and geometry information. Marin et al. [9] extract 7 features including intensity and geometry information, and then train a neural network classifier for vessel extraction. Roychowdhury et al. [10] extract the major vessel from the fundus images and use a Gaussian classifier for vessel segmentation with 8 features, which consists of intensity features and gradient features. Liskowski et al. [11] employ a deep neural network to extract vessel pixels from fundus images. Daniele et al. [12] use an U-Net [13] to achieve blood vessel segmentation. In unsupervised methods, the researchers try to discover latent vessel properties for vessel segmentation. Unsupervised methods can be further divided into multiscale approaches, matched filtering, vessel tracking, mathematical morphology and model based methods [5]. The multiscale approach introduced by [14] develops a vessel enhancement filter for vessel extraction with the analysis of image structure. The matched filtering method described by [15] employs different threshold probes to draw vessel pixels from the filtered images. The methodology based on vessel tracking [16] applies a wave propagation and traceback mechanism to label each pixel the likelihood of belonging to vessels in angiography images. The mathematical morphology with the extraction of vessel centerlines [17] is also developed to find the morphological characteristics of retinal blood vessels. Model based methods generally use geometric deformable models [18], parametric deformable models [19], vessel profile models [20] and active contour models [21] for blood vessel segmentation. Image matting means precisely segmenting the foregroundfrom an image.

Fig. 1. The process of image matting. (a) An image. (b) A trimap generatedby the user. The white, black and gray regions belong to the foreground,backgroundandunknownregions,respecti vely.(c)Aresultachievedby[22].

Generally image matting includes two mainsteps.Thefirststepisgeneratingauserspecified*trim ap*.Fig.1(b)givesanexampleofauserspecifiedtrimap.Tri mapis a hand-drawn segmented image, which is composed of theforeground,backgroundandunknownregions.Thes econdstepisemployingthemattingmodeltopickthepixe lsbelongingtotheforegroundfromtheunknownregions, onthe basis of the samples of foreground and background pixelsannotated by the observers. Fig.1(c) gives an exemplary resultachieved by [22]. Image matting is of great importance inmany applications, such as, image (or video) segmentation,videoproduction,newviewsynthesis,an dfilmmaking.Tothe best of our knowledge, image matting has rarely beenemployedpreviouslytoextractbloodvesselsfromfu ndusimage, and so far we have only found [23], which uses Hu'smoment features [9] and KNN matting [24] to perform bloodvesselsegmentation.Themajorreasonisthatgener atingauserspecified trimap for vessel segmentation is an extremely labo-rious and time-consuming task. In other words, it is not appro-priate to obtain a trimap manually for vessel segmentation. Inaddition, a proper image matting model needs to be designedcarefully to improve the vessel segmentation performance. Inorder to address these issues, region features of blood vesselsare employed to generate the trimap automatically. Then ahierarchicalimagemattingmodelisproposedtodrawth evessel pixels from the unknown regions. The proposed modelis evaluated on the public available datasets DRIVE, STARE,and CHASE DB1, which have been extensively used by otherscientists to develop their own methods. The segmentationperformance verifies the efficiency and effectiveness of theproposedhierarchicalimagemattingmodel.

Theremainderofthispaperisconstructedasfollows:Se ction II introduces some background knowledge of imagematting.SectionIIIdetailstheprocessofgenerating thetrimapofafundusimageautomatically,andthepropo sedhierarchical image matting model. Section IV introduces thepublic available datasets and the commonly used evaluationmetrics. The experimental results are detailed in Section V.TheconclusionisprovidedinSectionVI.

IMAGEMATTING

As aforementioned, image matting aims to accurately ex-tracttheforegroundgivenatrimapofanimage.Conc retely,the input image I can be considered as a linear aggregationofaforegroundimage$F$andabackgroundi mage$B$:

$$I=\alpha_z F+(1-\alpha_z)B \quad (1)$$

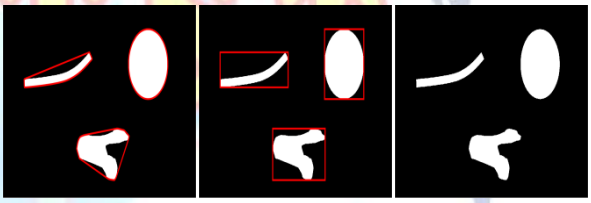

Fig. 2.An example to illustrate the bounding box and convex hull. (a) Theexemplary image. (b) The image for the illustration of bounding box. The redboxes are the bounding boxes. (c) The image for the illustration of convexhull.Theredpolygonsaretheconvexhulls.

where alpha matte $\alpha_z$indicates the probability of the fore-ground,whichrangesfrom0to1.

Afterobtainingtheuserspecifiedtrimap,toderiv ethe$\alpha_z$intheunknownregions,Chuang*etal.*[25]use ssetsof Gaussian distribution to obtain the color models of theforeground and background colors, and estimates the optimalalpha value by using a maximum-likelihood criterion. In [26],Levin *et al.* derives an effective objective function based onthe color smooth hypothesis, and employs this function toobtain the optimum of the alpha matte. Zheng *et al.* [22]performs image matting based on the local and global learningmethods. In

[27], Kaiming *et al.* solves a large kernel mattingLaplacian, and achieves a fast matting algorithm. In [28],Shahrian and Rajan use an effective cost function to selectthe optimal (*F, B*) couple for alpha matte evaluation. In [24],Qifeng *et al.* proposes a matting technique, and obtains anefficient result by leveraging on the preconditioned conjugategradient method. Shahrian *et al.* [29] expands the samplingrange of foreground and background regions, and collects arepresentativesetofsamplesforimagematting.In[30],Cho*etal.*presentsanimagemattingmethodtoasses salphamattesonsub-images of a light field image. Karacan [31] *et al.* proposesa sampling method, and employs a new distance metric toobtain the results of image matting. In [32], Cho *et al.* utilizesadeepconvolutionalneuralnetworktoachieveimagematting.Li *et al.* [33] designs a novel feature and three-layer graphframework for image matting. Aksoy *et al.* [34] designs aninter-pixel information flow to achieve image matting. In [35],Lee *et al.* performs parallel image matting on large imageswithmultipleprocessingcores.

METHODOLOGY

In this section, the process of generating the trimap of aninput fundus image automatically is introduced, followed bydetailingtheproposedhierarchicalimagematting model.

A. *TrimapGeneration*

Region features of blood vessels have been used for bloodvesselsegmentationandperformedwellonsegmentationaccuracy and computational efficiency [36]. In this paper, thetrimap of an input fundus image is generated automatically bybyutilizingregionfeaturesofbloodvessels.Thedefinitionsofregionsfeaturesaregivenasfollows:

Areaindicatesthenumberofpixelsintheregion.

- ***Bounding Box*** specifies the smallest rectangle incorpo-rating the region. Fig.2(b) gives an example of boundingbox.
- ***Extent*** represents the region proportion in the boundingbox.
- ***VRatio*** represents the ratio of the length to the width oftheboundingbox.
- ***Convex Hull*** means the smallest convex polygon incor-porating the region. Fig.2(c) gives an example of convexhull.
- ***Solidity*** represents the region proportion in the convexhull.

TABLEI

THEDEFAULTTHRESHOLDVALUESOFREGIONFEATURES:Extent,VRatio,SolidityANDTHEIRRECOMMENDEDRANGESUSEDINTHISWORK

Thresholdvalues	e_1	e_2	r	s
Defaultvalues	0.35	0.25	2.2	0.53
RecommendedRanges	[0.2,0.4]	[0.15,0.3]	[2,6]	[0.4,0.6]

The default threshold values of region features: *Extent*,*VRatio*, *Solidity* and their recommended ranges used in thiswork are reported in Table I. e_1 and e_2 are two thresholdvaluesof*Extent*featuresusedinthiswork;*r*isthethresholdvalue of *V Ratio* feature; *s* is the threshold value of *Solidity*feature.For*Area*feature,twothresholdvalues: $a_1=f_i2$and$a_2=f_i35$areusedinthiswork.f_i,calledtheinternalfactor, is calculated as $d\,\frac{max(h,w)}{}$, where d = 21 is roughlythe diameter of the biggest vessels in fundus images [37], *h*and*w*aretheheightandwidthofthefundusimage.

The proposed model is not sensitive to the above mentionedregionfeatures.Inotherwords,theseregionfeaturescanbeselectedinarelativelylargerangewithoutsacrificing theperformance.InSectionV(D)-"Sensitivityanalysisofthresholdvaluesofregionfeaturesandtheweightparameter",empiricalstudyisdirectedtodemonstratetheinsensitivityoftheproposedmodeltothethresholdvaluesofregionfeatures.

Creatingthetrimapoftheinputfundusimageautomaticallyincludestwomainsteps:1)ImageSegmentationand2)

VesselSkeleton Extraction. The process of trimapgeneration is giveninFig.3

1) Image Segmentation: Image segmentation aims to sepa-ratetheinputimageintothreeregions:thevessel(foreground),background and unknown regions. Firstly the enhanced vesselimageI_{mr}generatedbymorphologicalreconstruction[37]is segmented into three regions: the background regions (B),unknownregions(U)andpreliminaryvesselregions(V_1)

$$I_{mr} = \begin{cases} B & \text{if } 0 < I_{mr} < p_1 \\ U & \text{if } p_1 \leqslant I_{mr} < p_2 \\ V_1 & \text{if } p_2 \leqslant I_{mr} \end{cases} \quad (2)$$

where p1 = 0.2 and p2 = 0.35 restrict the unknown region as thin as possible in order to achieve the better matting result [28], [38]. In order to remove the noise regions in V1, the regions with Area > a1 in V1 are extracted firstly ($V * 1$). Then regions in $V * 1$ whose Extent ≤ e1 && V Ratio ≤ r && Solidity ≥ s are abandoned, resulting in the denoised preliminary vessel regions V2. Fig.4 gives an exemplary process of image segmentation.

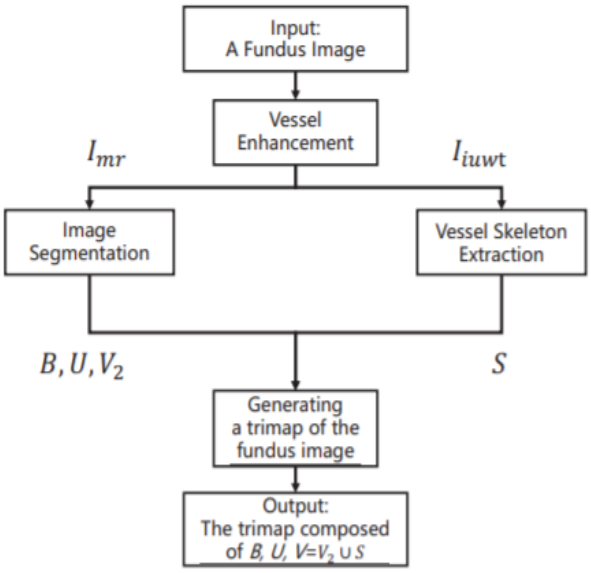

Fig. 3. The process of trimap generation. B represents the background regions; U represents the unknown regions; V2 represents the denoised preliminary vessel regions; S represents the skeleton of blood vessels; V represents the vessel regions.

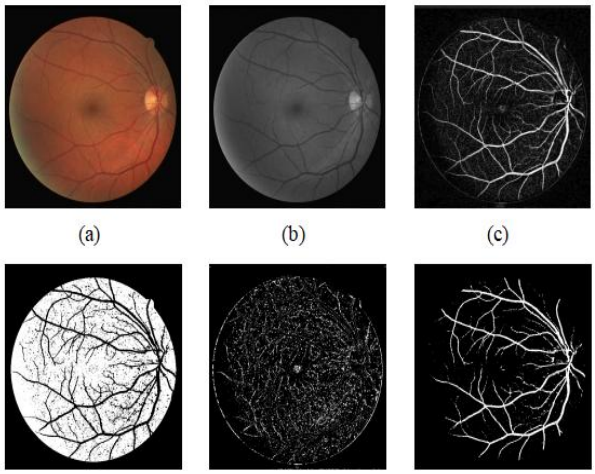

Fig.4.Imagesegmentation.(a)Thefundusimage$I$.(b)Thegreenplaneofthe fundus image I_g . (c) The enhanced vessel image I_{mr} . (d) The backgroundregions B. (e) The unknown regions U . (f) The denoised preliminary vesselregionsV_2

*Vessel Skeleton Extraction:*Vessel Skeleton Extractionaims to further distinguish the unknown regions and providemore information on blood vessels. In Section V(B)-"VesselSegmentation Performance", the effectiveness of vessel skele-ton extraction will be presented. Firstly, a segmented image $T$is generated by thresholding the enhanced vessel image I_{iuwt}generatedbytheisotropicundecimatedwaveletransform[39]

$$T = \begin{cases} 1 & I_{iuwt} > t \\ 0 & I_{iuwt} \leq t \end{cases} \quad (3)$$

where$t$=$Otsu(I_{iuwt})\varepsilon$,$\varepsilon$isset as0.03. Then$T$is dividedintothreeregionsaccordingtothe$Area$feature:

$$T = \begin{cases} T_1 & \text{if } 0 < Area < a_1 \\ T_2 & \text{if } a_1 \leq Area \leq a_2 \\ T_3 & \text{if } a_2 < Area \end{cases} \quad (4)$$

Invesselskeletonextraction,theregionsinT_3arepreservedwhiletheregionsinT_1areabandoned.Thentheregionsin T 2 with Extent > e2 && V Ratio ≤ r are preserved as T4. Finally skeleton extraction [40] is performed on the combined regions of T3 and T4 in order to obtain the vessel skeleton S. Fig.5 gives an exemplary process of vessel skeleton extraction.

After performing image segmentation and vessel skeleton extraction, the trimap of the input fundus image is generated (as shown in Fig.6(b)), which is composed of the background regions (B), unknown

regions (U) and vessel (or foreground) regions (V = V2 ∪ S).

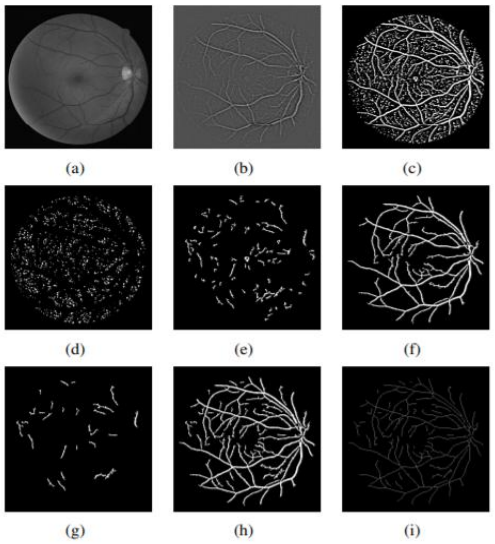

Fig. 5. Vessel skeleton extraction. (a) The green plane of the fundus image I_g. (b) The vessel enhanced image I_{iuwt}. (c) The binary image T. (d) The background regions T_1. (e) The candidate regions T_2. (f) The vessel regions T_3. (g) T_4: The preserved regions in T_2. (h) The combined regions of T_3 and T_4. (i) The vessel skeletons S.

B. Hierarchical Image Matting Model

Hierarchical image matting model is proposed to label the pixels in the unknown regions as vessels or background in an incremental way. Specifically, after stratifying the pixels in unknown regions (called unknown pixels) into m hierarchies by a hierarchical strategy, let u j i indicates the ith unknown pixel in the jth hierarchy, the segmented vessel image Iv(u j i) is modeled as follows:

$$I_v(u_i^j) = \begin{cases} 1 & \text{if } \beta(u_i^j, V) > \beta(u_i^j, B) \\ 0 & else \end{cases} \quad (5)$$

where β indicates the correlation function (depicted in Equation (8)). The implementation of the hierarchical image matting model consists of two main steps: Step 1 Stratifying the unknown pixels: Stratify pixels in the unknown regions into different hierarchies. Step 2 Hierarchical update: Assign new labels (V or B) to pixels in each hierarchy. The pseudocode implementing this model is shown in Algorithm 1.

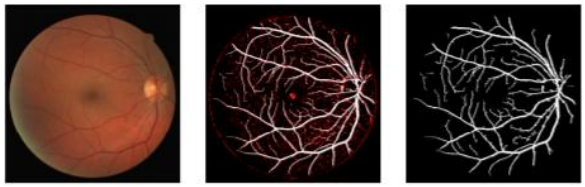

Fig. 6. (a) An input image. (b) A trimap generated by the proposed method. The white, black and red regions belong to the foreground, background and unknown regions, respectively. (c) The result achieved by the proposed hierarchical image matting model.

Algorithm 1: Implementing the hierarchical image matting model Input:
Trimap composed of B, U, V Output: The segmented vessel image Iv Step 1: Stratifying the unknown pixels: a) For i = 1, . . . , nU , set D(i) = di , where nU is the number of unknown pixels in U, di is the Euclidean distance between the ith unknown pixel and the closest vessel pixel in V , D is the set of di . b) Sort the unknown pixels in U in an ascending order according to the distances D , cluster the pixels with the same distance into one hierarchy, stratify the pixels into m hierarchies and denote them as an hierarchical order set: H = {H1, H2, . . . , Hm},
Hj = {u j i |i ∈ 1, 2, . . . , ni}, where ni is the number of unknown pixels in the jth hierarchy Hj .
Step 2: Hierarchical Update For j = 1, . . . , m, do For i = 1, . . . , ni , do a) Compute the correlations (Defined in Equation (8)) between u j i and its neighboring labelled pixels(vessel pixels and background pixels) included in a 9×9 grid. b) Choose the labelled pixel with the closest correlation, and assign its label (V or B) to u j i . end for end for Stratifying the unknown pixels: In this stage, the unknown pixels are stratified into different hierarchies. For the ith unknown pixel in U, its Euclidean distances with all vessel pixels in V are calculated first. Then the closest distance di is chosen and assigned to the ith unknown pixel. After that, the unknown pixels are stratified into different hierarchies according to the closest distances. The first hierarchy has the lowest value of the closest distance while the last hierarchy has the highest value of the closest distance. The unknown pixels reside in low hierarchy suggests that they are close to blood vessels; The unknown pixels stay in high hierarchy indicates that they are far away from blood vessels. Fig.7 gives an exemplary process of stratifying the unknown pixels. Correlation Function: In step 2 of Algorithm 1, given

an unknown pixel u j i and its neighboring labelled pixel k j l , a color cost function βc is defined to describe the fitness of u j i and k j l first:

βc(u j i , kj l) = | |cu j i − c k j l | | (6)

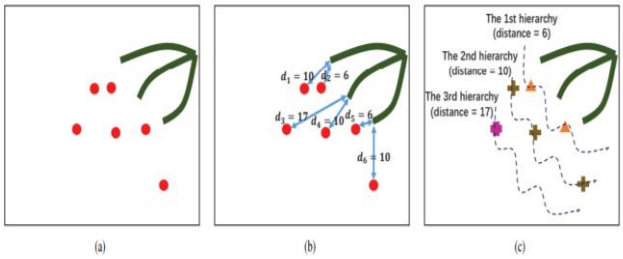

Fig. 7. An exemplary process of stratifying the unknown pixels. (a) An exemplary image (green pixels represent vessel pixels, red pixels represent unknown pixels). (b) Calculating the closest distance for each unknown pixel (d_i means the closest distance for the ith unknown pixel). (c) Stratifying unknown pixels into different hierarchies.

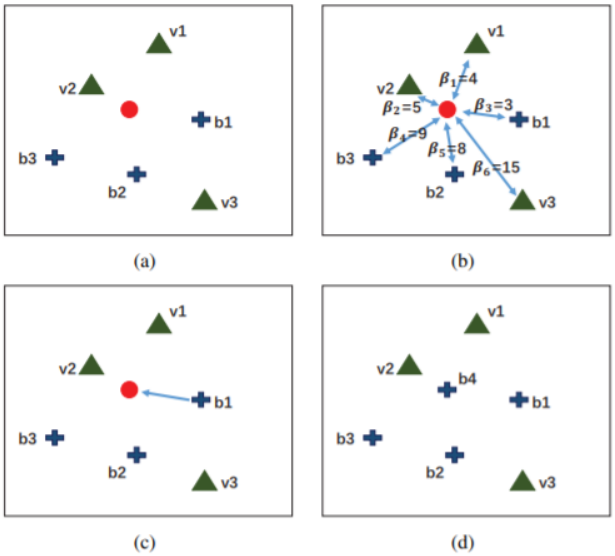

Fig. 8. An example for the illustration of assigning a label (V or B) to an unknown pixel. (a) An exemplary image (green triangles represent vessel pixels, blue pluses represent background pixels, red points represent unknown pixels). vi indicates the ith vessel pixel, bi indicates the ith background pixel. (b) Calculating the correlation functions between a unknown pixel and its neighboring labelled pixels (vessel pixels and background pixels) (βi means the correlation between the unknown pixel and the ith labelled pixel). (c) Assigning a label (V or B) to the unknown pixel. (d) The resultant image.

where $c_{u_i^j}$ and $c_{k_l^j}$ are intensity level of u_i^j and k_l^j in I_{mr}. A spatial cost function β_s is further defined:

$$\beta_s(u_i^j, k_l^j) = \frac{||x_{u_i^j} - x_{k_l^j}|| - x_{min}}{x_{max} - x_{min}} \quad (7)$$

where $x_{u_i^j}$ and $x_{k_l^j}$ are the spatial coordinates of u_i^j and k_l^j. The terms $x_{max} = max_j||x_{u_i^j} - x_{k_l^j}||$ and $x_{min} = min_j||x_{u_i^j} - x_{k_l^j}||$ are the maximum and minimum distance of the unknown pixel u_i^j to the labelled pixel k_l^j. The normalization factors x_{min} and x_{max} ensure that β_s is independent from the absolute distance.

Our final correlation function β is a combination of the color fitness and the spatial distance:

$$\beta(u_i^j, k_l^j) = \beta_c(u_i^j, k_l^j) + \omega\beta_s(u_i^j, k_l^j) \quad (8)$$

where ω is a weight parameter to trade off the color fitness and spatial distance. ω is assigned as 0.5 in our experiment. Generally a small β indicates that the labelled pixel has a close correlation with the unknown pixel, and they have a high probability of belonging to the same class. Hierarchical Update: After performing initialization with the hierarchical strategy, in each hierarchy, the correlations between each unknown pixel and its neighboring labelled pixels (vessel pixels and background pixels) included in a 9 × 9 grid are computed. Then the labelled pixel with the closest correlation is chosen, and its label is assigned to the unknown pixel. After all unknown pixels in one hierarchy are updated, they are used for updating the next hierarchy. The unknown pixels are updated from the first hierarchy to the last hierarchy. An example to illustrate the process of updating unknown pixels in one hierarchy is shown in Fig.8.

C. Postprocessing Since some non-vessel regions may still exist in the final segmented vessel image Iv, the regions whose Area < a2 && Extent > e2 && V Ratio < r in Iv are abandoned to remove these non-vessel regions.

DATASETS AND EVALUATION METRICS

In this section, three publicly available datasets are introduced. These datasets have been extensively used by other scientists to develop their own methods. Then some commonly used evaluation metrics are presented, which are also utilized in our experiment to make a comparison between the proposed model with several other approaches. A. Datasets The proposed model is evaluated on three standard datasets: DRIVE [6], STARE [15] and CHASE DB1 [37]. DRIVE1 consists of 40 fundus images. These images are taken by a Canon camera at 45◦ field of view (FOV). Each image is of 584×565 pixels. The DRIVE dataset is separated into two sets: a training set and a test set each including 20

fundus images. The training set is marked by two observers; The test set is marked by two independent observers.

TABLE II
COMPARISON BETWEEN THE PROPOSED MODEL AND OTHER METHODS

Test Datasets	DRIVE					STARE					
Methods	Acc	AUC	Se	Sp	Time	Acc	AUC	Se	Sp	Time	System
Supervised Methods											
Staal *et.al* [6]	0.944	-	-	-	15min	0.952	-	-	-	15min	1.0 GHz, 1-GB RAM
Soares *et.al* [7]	0.946	-	-	-	~3min	0.948	-	-	-	~3min	2.17 GHz, 1-GB RAM
Lupascu *et.al* [8]	0.959	-	0.720	-	-	-	-	-	-	-	-
Marin *et.al* [9]	0.945	0.843	0.706	0.980	~90s	0.952	0.838	0.694	0.982	~90s	2.13 GHz, 2-GB RAM
Roychowdhury *et.al* [10]	0.952	0.844	0.725	0.962	3.11s	0.951	0.873	0.772	0.973	6.7s	2.6 GHz, 2-GB RAM
Liskowski *et.al* [11]	0.954	0.881	0.781	0.981	-	0.973	0.921	0.855	0.986	-	NVIDIA GTX Tian GI
Daniele *et.al* [12]	0.956	0.875	0.767	0.983	15.31s	0.972	0.896	0.806	0.986	23.2s	NVIDIA Tian XP GP
Unsupervised Methods											
Hoover *et.al* [15]	-	-	-	-	-	0.928	0.730	0.650	0.810	5min	Sun SPARCstation 2
Mendonca *et.al* [17]	0.945	0.855	0.734	0.976	2.5min	0.944	0.836	0.699	0.973	3min	3.2 GHz, 980-MB RA
Lam *et.al* [41]	-	-	-	-	-	0.947	-	-	-	8min	1.83 GHz, 2-GB RAM
Al-Diri *et.al* [19]	-	-	0.728	0.955	11min	-	-	0.752	0.968	-	1.2 GHz
Lam and Yan *et.al* [20]	0.947	-	-	-	13min	0.957	-	-	-	13min	1.83 GHz, 2-GB RAM
Perez *et.al* [42]	0.925	0.806	0.644	0.967	~2min	0.926	0.857	0.769	0.944	~2min	Parallel Cluster
Miri *et.al* [43]	0.943	0.846	0.715	0.976	~50s	-	-	-	-	-	3 GHz, 1-GB RAM
Budai *et.al* [44]	0.957	0.816	0.644	0.987	-	0.938	0.781	0.580	0.982	-	2.3 GHz, 4-GB RAM
Nguyen *et.al* [45]	0.941	-	-	-	2.5s	0.932	-	-	-	2.5s	2.4 GHz, 2-GB RAM
Yitian *et.al* [21]	0.954	0.862	0.742	0.982	-	0.956	0.874	0.780	0.978	-	3.1 GHz, 8-GB RAM
Annunziata *et.al* [46]	-	-	-	-	-	0.956	0.849	0.713	0.984	<25s	1.9 GHz, 6-GB RAM
Orlando *et.al* [47]	-	0.879	0.790	0.968	-	-	0.871	0.768	0.974	-	2.9 GHz, 64-GB RAM
Proposed	**0.960**	**0.858**	**0.736**	**0.981**	**10.72s 6.25s**	**0.957**	**0.880**	**0.791**	**0.970**	**15.74s 9.66s**	**2.5 GHz, 4-GB RAM NVIDIA GTX Tian G**

STARE2 consists of 20 fundus images. These images are taken by a TopCon camera at 35◦ FOV. Each image is of 605× 700 pixels. The STARE dataset is marked by two independent observers. CHASE DB13 consists of 28 fundus images acquired from multiethnic school children. These images are captured by a Nidek camera at 30◦ FOV. Each image is of 960×999 pixels. The CHASE DB1 is marked by two independent observers. For the DRIVE, STARE and CHASE DB1 datasets, the manual segmentations of the first observer are used in this work, which is a common choice for these datasets [5], [11], [21], [46]. B. Evaluation Metrics For vessel segmentation, each pixel is classified as vessels or background, thereby resulting in four events: two correct (true) classifications and two incorrect (false) classifications (as shown in Table III).algorithms, three commonly used metrics are applied

TABLE III
FOUR EVENTS OF VESSEL CLASSIFICATION

	Vessel present	Vessel absent
Vessel detected	True Positive (TP)	False Positive (FP)
Vessel not detected	False Negative (FN)	True Negative(TN)

To evaluate the performance of the vessel segmentation

[2]http://www.ces.clemson.edu/ ahoover/stare/
[3]https://blogs.kingston.ac.uk/retinal/chasedb1/

$$Sensitivity = \frac{TP}{TP + FN}$$

$$Specificity = \frac{TN}{TN + FP}$$

$$Accuracy = \frac{TP + TN}{TP + TN + FP + FN}$$

Sensitivity (Se) and Specificity (Sp) reflect the algorithm's ability to detect vessel pixels and background pixels. Accuracy (Acc) is a global measure of classification performance combing both Se and Sp. The performance of the vessel segmentation method is also measured by the area under a receiver operating characteristic (ROC) curve (AUC). The conventional AUC is calculated from a number of operating points, and normally used to evaluate the balanced data classification problem. However, in practice the researchers need to select an operating point to compare their method with other methods. In addition blood vessel segmentation is an imbalanced classification problem, in which the number of vessel pixels is much smaller than the number of background pixels. In order to evaluate the performance of blood vessel segmentation properly, AUC = (Se + Sp)/2 [21], [48] is applied to indicate the overall vessel segmentation performance, which is suitable to describe the overall performance of imbalanced data classification problem and specifically for the case when only one operating point is used. The calculation time of extracting blood vessels from a fundus images is also stored. In addition, the Dice scores (D) [21] is applied to evaluate the similarity between the manual segmentations and results of vessel segmentation algorithms: $D = 2(M \cap S)/(M + S)$,where M represents the manual segmentation and S represents the segmentation result

TABLE IV
THE SEGMENTATION PERFORMANCE OF THE PROPOSED MODEL ON THREE TEST DATASETS

Dataset	Method	Acc	AUC	Se	Sp	D	Time(s)
DRIVE	Trimap (Treating the unknown regions as background regions)	0.959	0.833	0.679	0.986	0.765	5.841
	The proposed hierarchical matting model without vessel skeleton extraction	0.960	0.837	0.688	0.986	0.771	11.959
	The proposed hierarchical matting model with vessel skeleton extraction	0.960	0.859	0.736	0.981	0.780	10.720
STARE	Trimap (Treating the unknown regions as background regions)	0.958	0.853	0.728	0.977	0.737	7.741
	The proposed hierarchical matting model without vessel skeleton extraction	0.959	0.862	0.748	0.976	0.745	16.563
	The proposed hierarchical matting model with vessel skeleton extraction	0.957	0.881	0.791	0.970	0.752	15.740
CHASE_DB1	Trimap (Treating the unknown regions as background regions)	0.948	0.771	0.565	0.977	0.598	21.088
	The proposed hierarchical matting model without vessel skeleton extraction	0.954	0.789	0.597	0.981	0.650	60.847
	The proposed hierarchical matting model with vessel skeleton extraction	0.951	0.815	0.657	0.973	0.665	50.710

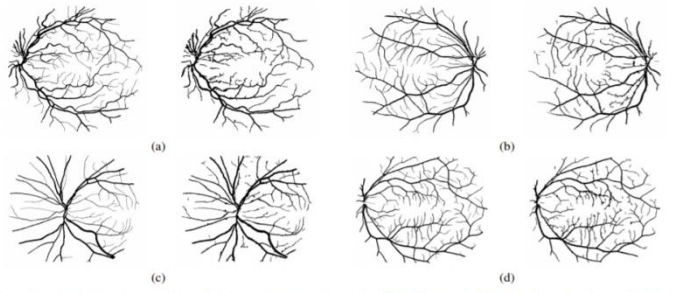

Fig. 9. Ground truth (left) and segmentation result (right): (a) and (b) are the images from DRIVE dataset, (c) and (d) are the images from the STARE dataset

Vessel Segmentation Performance The segmentation performance of the proposed method on three public available datasets is given in Table IV. Fig.9 presents Some exemplary segmentation results. When treating

the unknown regions as background regions, trimap can achieve segmentation results of Acc = 0.959, AUC = 0.833, Se = 0.679, Sp = 0.986, D = 0.765 on the DRIVE dataset, Acc = 0.958, AUC = 0.853, Se = 0.728, Sp = 0.977, D = 0.737 on the STARE dataset, Acc = 0.948, AUC = 0.771, Se = 0.565, Sp = 0.977, D = 0.598 on the CHASE DB1 dataset, respectively. These segmentation performances show that trimap can already have fairly good segmentation performance, which indicates that the selection of region features is effective in segmenting blood vessels. However, the performance is still not satisfactory enough when compared with other methods. A hierarchical image matting model is proposed to improve the segmentation performance. AUC = 0.837, 0.862, 0.789 achieved by the proposed hierarchical matting model on the DRIVE, STARE and CHASE DB1 are 0.4%, 0.9% and 1.8% higher than that of trimap, respectively. Se = 0.688, 0.748, 0.597 achieved by the proposed hierarchical matting model on the DRIVE, STARE and CHASE DB1 are 0.9%, 2% and 2.8% higher than that of trimap, respectively. In addition, D = 0.771, 0.745, 0.650 obtained by the proposed hierarchical matting model on the DRIVE, STARE and CHASE DB1 are 0.6%, 0.8% and 5.2% higher than that of trimap, respectively. The segmentation performance can be further improved by applying vessel skeleton extraction. From Table IV, it can be observed that compared with the proposed image matting model without vessel skeleton extraction, the matting model with vessel skeleton extraction can achieve 4.8% increase of Sensitivity, 2.2% increase of AUC and 0.9% increase of D on the DRIVE dataset, 4.3% increase of Sensitivity, 1.9% increase of AUC and 0.7% increase of D on the STARE dataset, 6% increase of Sensitivity, 2.8% increase of AUC and 1.5% increase of D on the CHASE DB1 dataset, which demonstrates the effectiveness of applying the mechanism of vessel skeleton extraction

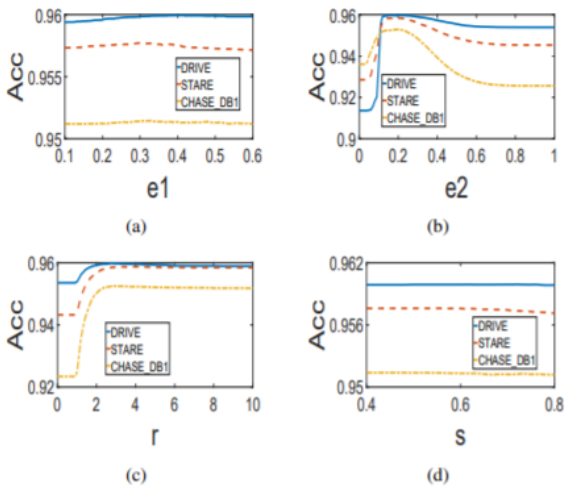

Fig. 10. Sensitivity analysis of threshold values of region features used in the work. (a) Variations in mean segmentation accuracy by varying e_1 when $r = 2.2$, $s = 0.53$, $e_2 = 0.25$. (b) Variations in mean segmentation accuracy by varying e_2 when $r = 2.2$, $e_1 = 0.35$, $s = 0.53$. (c) Variations in mean segmentation accuracy by varying r when $e_1 = 0.35$, $s = 0.53$, $e_2 = 0.25$. (d) Variations in mean segmentation accuracy by varying s when $r = 2.2$, $e_1 = 0.35$, $e_2 = 0.25$.

Comparison with image matting models The effectiveness of the proposed model in blood vessel segmentation has been validated through previous experiments. In order to further verify the effectiveness of our model, the proposed model is compared with eight other state-ofart image matting models: Anat Model [26], Zheng Model [22], Shahrian Model [28], Improving Model [29], Karacan Model [31], Cho Model [32], Li Model [33] and Aksoy Model [34]. The segmemtation results of these models on the DRIVE, STARE, and CHASE DB1 datasets are given in Table V. The proposed model outperforms these image matting models in terms of Acc and Sp in the DRIVE, STARE and CHASE DB1 datasets.

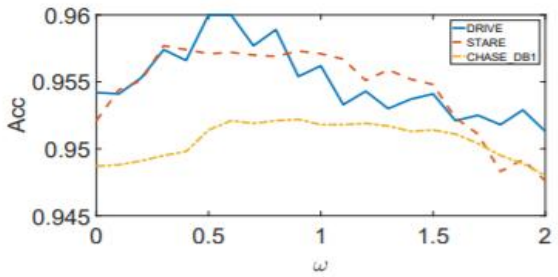

Fig. 11. Variations in mean segmentation accuracy by varying ω.

Sensitivity analysis of threshold values of region features and the weight parameter The default threshold values of region features: e1 = 0.35, r = 2.2, s = 0.53, e2 = 0.25 are applied in this experiment. To demonstrate the insensitivity of the proposed model to these threshold values, the variations in Acc by varying e1, e2, r and s are given in Fig.10.(a), (b), (c) and (d).

From Fig.10, it can be observed that the proposed model can maintain high segmentation accuracy on the DRIVE, STARE and CHASE DB1 datasets as e1 varies in [0.2, 0.6] or e2 varies in [0.15, 0.3]; For r and s, the proposed model can maintain high segmentation accuracy as r varies in [2, 10] or s varies in [0.4, 0.8]. In addition, the variation in Acc by varying ω is given in Fig.11. From Fig.11, it can be observed that the proposed model can maintain high segmentation accuracy on the DRIVE, STARE and CHASE DB1 datasets as ω varies in [0.4, 0.8]. From the above observation, it can be seen that the proposed model is not sensitive to these threshold values of region features and the weight parameter ω

VI. CONCLUSION Image matting means precisely segmenting the foreground from an image, which is crucial in many important applications. However, to the best of our knowledge, image matting has rarely been employed previously to extract blood vessels from fundus image. The major reason may be that generating a user specified trimap for vessel segmentation is an extremely laborious and time-consuming task. In addition, a proper image matting model needs to be designed carefully to improve the vessel segmentation performance. In order to address these issues, region features of blood vessels are first employed to generate the trimap automatically. Then a hierarchical image matting model is proposed to extract the vessel pixels from the unknown regions. More specifically, a hierarchical strategy is integrated into the image matting model for blood vessel segmentation. The proposed model is very efficient and effective in blood vessel segmentation, which achieves a segmentation accuracy of 96.0%, 95.7% and 95.1% on three public available datasets with an average time of 10.72s, 15.74s and 50.71s, respectively. The experimental results show that it is a very competitive model compared with many other segmentation approaches.

ACKNOWLEDGMENT This research work was supported by Guangdong Key Laboratory of Digital Signal and Image Processing, the National Natural Science Foundation of China under Grant (61175073, 61300159, 61332002, 51375287), the Natural Science Foundation of Jiangsu Province of China under grant SBK2018022017.

REFERENCES

[1] S. Abbasi-Sureshjani, M. Favali, G. Citti, A. Sarti, and B. M. T. H. Romeny, "Curvature integration in a 5d kernel for extracting vessel connections in retinal images," IEEE Transactions on Image Processing, vol. PP, no. 99, pp. 1–1, 2017.

[2] J. J. Kanski and B. Bowling, Clinical Ophthalmology: A Systematic Approach. Elsevier Health Sciences, 2011.

[3] M. W. Law and A. C. Chung, "Segmentation of intracranial vessels and aneurysms in phase contrast magnetic resonance angiography using multirange filters and local variances," IEEE Transactions on image processing, vol. 22, no. 3, pp. 845–859, 2013.

[4] Y. Cheng, X. Hu, J. Wang, Y. Wang, and S. Tamura, "Accurate vessel segmentation with constrained b-snake," IEEE Transactions on Image Processing, vol. 24, no. 8, pp. 2440–2455, 2015.

[5] M. M. Fraz, P. Remagnino, A. Hoppe, B. Uyyanonvara, A. R. Rudnicka, C. G. Owen, and S. A. Barman, "Blood vessel segmentation methodologies in retinal images–a survey," Computer Methods and Programs In Biomedicine, vol. 108, no. 1, pp. 407–433, 2012.

[6] J. Staal, M. D. Abramoff, M. Niemeijer, M. A. Viergever, and B. van ` Ginneken, "Ridge-based vessel segmentation in color images of the retina," IEEE Transactions on Medical Imaging, vol. 23, no. 4, pp. 501– 509, 2004.

[7] J. V. Soares, J. J. Leandro, R. M. Cesar, H. F. Jelinek, and M. J. Cree, "Retinal vessel segmentation using the 2-d gabor wavelet and supervised classification," IEEE Transactions on Medical Imaging, vol. 25, no. 9, pp. 1214–1222, 2006.

[8] C. A. Lupascu, D. Tegolo, and E. Trucco, "Fabc: Retinal vessel segmentation using adaboost," IEEE Transactions on Information Technology in Biomedicine, vol. 14, no. 5, pp. 1267–1274, 2010.

[9] D. Mar´ın, A. Aquino, M. E. Gegundez-Arias, and J. M. Bravo, "A new ´ supervised method for blood vessel segmentation in retinal images by using gray-level and moment invariants-based features," IEEE Transactions on Medical Imaging, vol. 30, no. 1, pp. 146–158, 2011.

[10] S. Roychowdhury, D. D. Koozekanani, and K. K. Parhi, "Blood vessel segmentation of fundus images by major vessel extraction and subimage classification," IEEE Journal of Biomedical and Health Informatics, vol. 19, no. 3, pp. 1118–1128, 2015.

[11] P. Liskowski and K. Krawiec, "Segmenting retinal blood vessels with deep neural networks," IEEE Transactions on Medical Imaging, vol. 35, pp. 1–1, 2016.

[12] O. S. Daniele Cortinovis, "Retina blood vessel segmentation with a convolution neural network (u-net)," available: https://github.com/ orobix/retina-unet, 2016.

[13] O. Ronneberger, P. Fischer, and T. Brox, "U-net: Convolutional networks for biomedical image segmentation," in International Conference on Medical image computing and computer-assisted intervention. Springer, 2015, pp. 234–241.
[14] A. F. Frangi, W. J. Niessen, K. L. Vincken, and M. A. Viergever, "Multiscale vessel enhancement filtering," in International Conference on Medical Image Computing and Computer-Assisted Intervention. Springer, 1998, pp. 130–137.
[15] A. Hoover, V. Kouznetsova, and M. Goldbaum, "Locating blood vessels in retinal images by piecewise threshold probing of a matched filter response," IEEE Transactions on Medical Imaging, vol. 19, no. 3, pp. 203–210, 2000.
[16] F. K. Quek and C. Kirbas, "Vessel extraction in medical images by wavepropagation and traceback," IEEE Transactions on Medical Imaging, vol. 20, no. 2, pp. 117–131, 2001.
[17] A. M. Mendonca and A. Campilho, "Segmentation of retinal blood vessels by combining the detection of centerlines and morphological reconstruction," IEEE Transactions on Medical Imaging, vol. 25, no. 9, pp. 1200–1213, 2006.
[18] K. Sum and P. Y. Cheung, "Vessel extraction under non-uniform illumination: A level set approach," IEEE Transactions on Biomedical Engineering, vol. 55, no. 1, pp. 358–360, 2008